

# Comparative study of coherent terahertz emission from Fe/Pt ferromagnetic heterostructures

Xiao-Peng He (贺小鹏)<sup>1</sup>, Pan-Hui Huang (黄潘辉)<sup>1</sup>, Xiao-Yu Yang (杨晓钰)<sup>1</sup>,  
Zuan-Ming Jin (金钻明)<sup>2</sup>, Shi-Tao Lou (楼柿涛)<sup>1,\*</sup>, Xiao-Lei Zhang (张晓磊)<sup>1,\*\*</sup>,  
and Qing-Yuan Jin (金庆原)<sup>1,3</sup>

<sup>1</sup>State Key Laboratory of Precision Spectroscopy, School of Physics and Material Science, East China Normal University, Shanghai 200062, China

<sup>2</sup>Department of Physics, Shanghai University, Shanghai 200444, China

<sup>3</sup>Shanghai Engineering Research Center of Ultra-Precision Optical Manufacturing and Key Laboratory of Micro and Nano Photonic Structures (Ministry of Education), Department of Optical Science and Engineering, Fudan University, Shanghai 200433, China

\*Corresponding author: stlou@admin.ecnu.edu.cn; \*\*corresponding author: xlzhang@admin.ecnu.edu.cn

Received January 26, 2019; accepted May 13, 2019; posted online July 10, 2019

The ultrafast spin dynamic of in-plane magnetized Fe/Pt films was investigated by terahertz emission spectroscopy. The amplitude of the emitted terahertz wave is proportional to the intensity of the exciting laser beams. Both the amplitude and polarity of the terahertz wave can be adjusted by modifying the external magnetic field. The dependency of the amplitude on external magnetic fields is coincident to the hysteresis loops of the sample. Also, the polarity of the terahertz wave is reversed, as the magnetization orientation is reversed. The super-diffusive transient spin current with an inverse spin Hall effect is attributed to the main mechanism of the terahertz emission.

OCIS codes: 160.3820, 310.6845, 320.2250.

doi: 10.3788/COL201917.081601.

Since the 2000s, terahertz (THz) technology has continued to have attention not only in basic research, but also in its extensive application research, such as food safety, chemical detection, material testing, and biomedicine<sup>[1-3]</sup>. Ultrafast spin dynamics in magnetic materials have potential applications in ultrafast spin control, spintronics, and quantum computing<sup>[4-5]</sup>. THz time domain spectroscopy (TDS)<sup>[6]</sup> allows the probing of charge carrier dynamics, since its frequency range corresponds to the characteristic energy of electronic intra-band transitions<sup>[10,11]</sup>.

Furthermore, it has been found that femtosecond lasers interacting with ferromagnetic (FM) materials, such as Fe, Co, and Ni, can produce THz radiation<sup>[12-14]</sup>. In 2004, Beaurepaire *et al.* found that the laser inducing ultrafast demagnetization of FM film emits THz pulses<sup>[13]</sup>. In 2007, Chau *et al.* found that the direction of the external magnetic field can influence the intensity of the THz pulse<sup>[15]</sup>. In 2013, Kampfrath *et al.* measured the THz radiation from FM iron thin film samples with a non-magnetic (NM) capping layer excited by a femtosecond pulse laser. They put forward a point that the THz wave is produced by electric dipole oscillation in the NM capping layer, which is converted from the spin current flow in the FM layer by the inverse spin Hall effect (ISHE)<sup>[16]</sup>. In 2015, Huisman *et al.* measured the time resolved magneto-optical Kerr effect (MOKE) and the THz time domain spectrum of pure Co and GdFeCo alloys. They found that the THz emission spectroscopy had a good qualitative and quantitative agreement with the MOKE<sup>[17]</sup>.

However, the mechanism of THz radiation from magnetic film is still unclear. Both the demagnetization effect of FM materials and the ISHE involve hot electrons<sup>[16,17]</sup>, which are excited by photons and interact with the lattice, phonons, and other electrons, and loss of memory for the polarization of the pump laser. Here, THz radiation from Fe/Pt films was investigated with intensity and the orientation of the sample and the magnetic field.

In our work, ultrathin Fe/Pt films are prepared on a glass substrate by magnetron sputtering<sup>[18]</sup> in an ultra-high vacuum chamber. The substrate is the Eagle2000 (Corning Company) glass with a thickness of 0.7 mm. The growth rate of both iron and platinum is 0.05 nm/s. The platinum was deposited on the iron layer as a capping layer to protect the iron from oxidization. The direction of the magnetic moment of the sample is in the plane of the sample surface.

The schematic of our experiments is shown in Fig. 1. A femtosecond pulse laser beam (center wavelength of 800 nm, duration of 120 fs, repetition rate of 1 kHz) is split into two beams: the first beam with 70% power is used for pumping the sample Fe/Pt, and the other beam with 30% power is used as a probe beam to detect the THz fields after traveling along a variable delay line. A silicon wafer is used to block the 800 nm near infrared beam. Probe pulses are coupled with the THz fields within a ZnTe crystal with a polarization 45° in the horizontal direction. The probe beam is split into two components with horizontal and vertical polarization, which were detected by two photodiodes (PDs) of a balanced detector

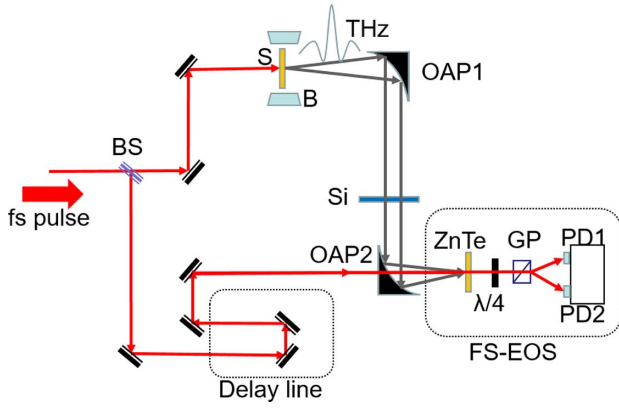


Fig. 1. Schematic of the THz TDS. BS, beam splitting mirror; S, Fe/Pt film; B, external magnetic field; OAP, off-axis parabolic mirror; Si, silicon wafer; FS-EOS, free-space electric-optical sampling consisting of an electro-optic crystal (ZnTe), a quarter-wave plate ( $\lambda/4$ ), a Glen prism (GP), and two balanced photodiodes (PD1 and PD2).

(PD1 and PD2), respectively. The THz field changes the polarization of the probe beam in the ZnTe crystal with the Pockels effect, and consequently changes the photocurrent of the diodes. The differential signal of the balanced detector is linearly proportional to the electric field of the THz waveform.

Figure 2(a) shows a typical THz waveform  $E(t)$  radiated from a heterostructure sample of Fe(7 nm)/Pt(4 nm). The laser pulse energy is 1.4 mJ with a beam spot diameter of 6 mm. The sample is applied with saturating magnetic fields of  $-B = -200$  Oe. Figure 2(b) corresponds to the normalized THz amplitude spectra. The central frequency of the radiation THz signal is about 0.4 THz, and the frequency range of Fe(7 nm)/Pt(4 nm) is 0.1–2 THz. The detected THz waveform is independent of the polarization of the incident laser; thus, optical rectification can be ruled out. The peak amplitude of the THz waveform varies as the intensity of the pump pulse increases, as is shown in the inset of Fig. 2(b). The black point is the peak-to-peak values of the THz signal, and the red line is a linear fitting to the data. It can be found that the intensity of THz radiation is proportional to the fluence of the pump pulse. This is more evident for ruling out the mechanism of optical rectification<sup>[19]</sup>.

Figure 3(a) shows the THz radiation measured in a saturating magnetic field of  $+B = +200$  Oe. The phase of the THz pulse is inverted as the orientation of  $B$  is reversed, which confirms that the THz emission is strongly correlated to the spin ordering. There are mainly two mechanisms of THz emission from the FM thin layer sample. First, the pump pulses produce a sub-picosecond demagnetization, which is equal to magnetic dipole moment radiation<sup>[13,20]</sup>, and the electric field emitted in the far field is given as the following:

$$E_y(t) = \frac{u_0}{4\pi^2 r} \frac{\partial^2 M_x}{\partial t^2}(t - r/c), \quad (1)$$

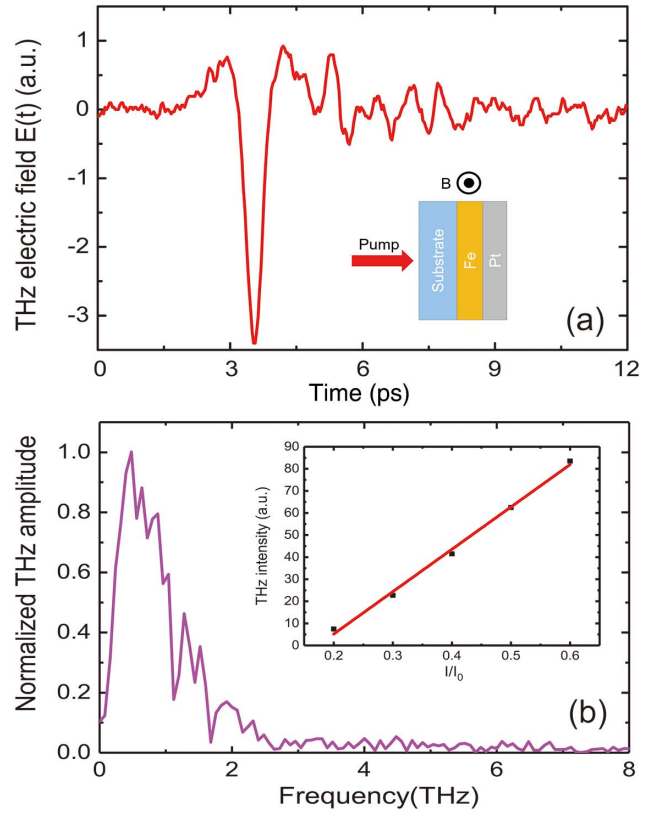


Fig. 2. (a) THz emission from a sample of Fe(7 nm)/Pt(4 nm) with laser pulse energy of 1.4 mJ under a beam spot diameter of 6 mm in a saturating magnetic field of  $-B = -200$  Oe. (b) The normalized THz amplitude spectra of Fe(7 nm)/Pt(4 nm) thin film. The central frequency of the radiation THz signal is about 0.4 THz, and the frequency range of Fe(7 nm)/Pt(4 nm) is 0.1–2 THz. Inset: the peak amplitude of the wave form varies as the intensity of the pump pulse changes. The black point is the peak-to-peak value (normalization) of the THz signal, and the red line is the linear fitting data. The intensity of THz radiation is proportional to the intensity of the pump pulse.

where  $r$  is the distance to the dipole.  $M_x$  is the magnetic moment in the  $x$  direction, which means the horizontal direction in our experiment.  $E_y$  is the electric field in the  $y$  direction (vertical direction).  $u_0$  is the vacuum magnetic permeability. Secondly, the laser excitation of free-electron gas in a magnetic field could also induce the electric dipole radiation of THz emission<sup>[17,21]</sup>. A near infrared femtosecond pulse excites the film. Due to different transport properties for spin channels in the FM layer, an ultrafast spin current is launched into the NM layer, which is converted into a transverse charge current by ISHE<sup>[22]</sup>. Finally, the charge current radiates the THz pulse. Though both the demagnetization effect of FM materials and the ISHE involve hot electrons, demagnetization directly results from the reversal of the hot electron's spin. However, the ISHE results from the diffusion of the hot electrons. With the help of spin, the diffusing hot electrons build up a charge current. If the THz emission is generated by ISHE, as the sample is inverted, the direction of a spin current between adjacent

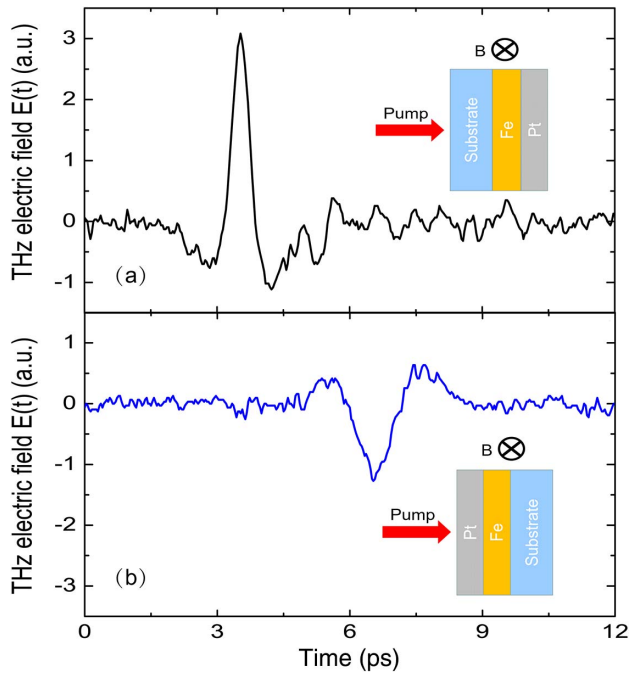


Fig. 3. (a) THz emission from a sample of Fe(7 nm)/Pt(4 nm) with a saturating magnetic field of  $+B = +200$  Oe. The phase of the THz pulse is inverted as the orientation of  $B$  is reversed. (b) The same sample in (a) is turned over as shown in (b) inset, where the polarity of THz emission has been inverted. That means THz emission can be reliably attributed mainly to the super-diffusive transient spin current with ISHE.

layers should be reversed. Therefore, the polarity of the THz radiation will be inverted as well<sup>[23]</sup>.

Figure 3(b) shows the THz wave form, measured as the sample is turned over  $180^\circ$  with a magnetic field of  $+B = +200$  Oe. It is obvious that the polarity of THz emission is inverted. Due to dispersion of the refractive index in glass between the near infrared and THz wave, we found that the time delay of the THz waveform is different. There are a couple of possible factors leading to the decrease of the THz waveform. The first factor is the absorption of the Pt and glass. In previous experiments, Pt has a strong absorption of laser at 800 nm. Pt with 2 nm can absorb 10% of the laser energy, and Pt with 7 nm can absorb about 55%. The glass can absorb about 68% of the energy of the THz wave. As shown in the Fig. 3(b), when the intensity of the 800 nm laser pulse decreases, the amplitude of the THz waveform decreases linearly. The second possibility is the superposition of magnetic dipole radiation. Though the sample is turned around, the saturating magnetic field maintains the same direction of magnetization, which means that the magnetic momentum maintains the same direction. Therefore, THz radiation by demagnetization will not change its phase. It should be noted that the superposition of the contribution of this part also leads to the decrease of the THz amplitude. However, the contribution of this part is pretty small. In conclusion, the observed THz emission can be reliably attributed mainly to the super-diffusive transient spin current with ISHE.

The spin polarized electrons are closely related to the magnetic moment of the sample, as mentioned before. We can also control the magnetic moment of the sample by modulating the external magnetic field and then controlling the spin current. The THz waveforms from Fe(5 nm)/Pt(2 nm) are obtained with different external magnetic fields changing from  $-100$  to  $+100$  Oe, as shown in Fig. 4(a). It can be found that the THz radiation amplitude decreases with the external magnetic field changing from  $-100$  to  $+30$  Oe. When the external magnetic field exceeds  $+30$  Oe, the polarity of the THz radiation reverses, and the amplitude of the THz pulse increases with the increase of the magnetic field. When the external magnetic field reaches  $+80$  Oe, the THz signal intensity is maximum and will not change thereafter. THz waveforms are also measured with an external magnetic field from  $+100$  to  $-100$  Oe. The dependency of the THz signal amplitude on the external magnetic field is plotted as red points in Fig. 4(b). However, the center frequency is about 0.6 THz, and the full width at half-maximum is about 0.6 THz, both of which are independent of the external magnetic field. The MOKE is plotted as the blue points in Fig. 4(b). It is important to see that the two curves coincide very well. The coercive field of our Fe(5 nm)/Pt(2 nm) sample is about 30 Oe, which is

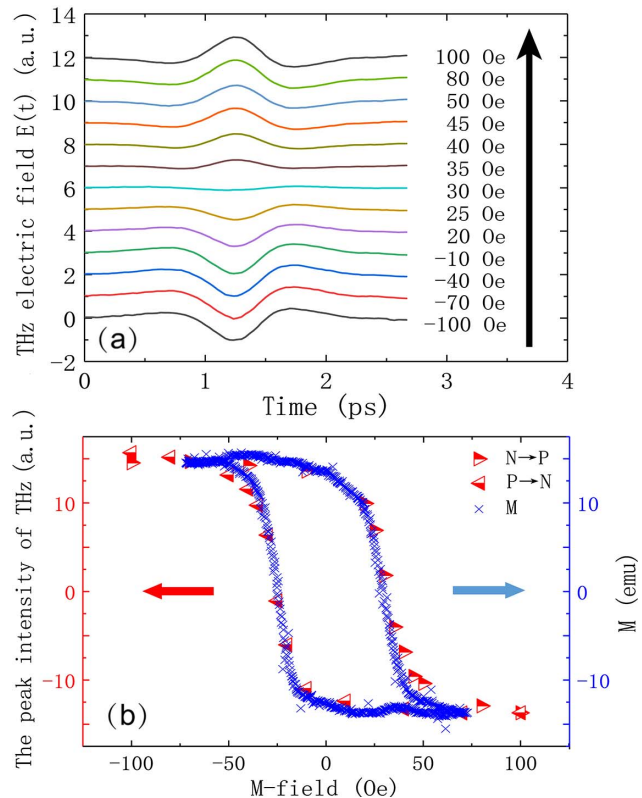


Fig. 4. (a) Electric field of the emitted THz radiation from Fe(5 nm)/Pt(2 nm) as a function of time with different external magnetic fields from  $-100$  to  $+100$  Oe. The traces are vertically shifted with respect to each other. (b) Amplitude (red point) of the THz signal with different external magnetic fields and MOKE signal of Fe(5 nm)/Pt(2 nm) (blue point).

basically the same value of the applied magnetic field required to reverse the polarity of the THz signal. The coincidence is also found in the other samples, such as Fe(2 nm)/Pt(2 nm) and Fe(7 nm)/Pt(2 nm). The magnetic moment of the sample increases with the external magnetic field intensified, which leads to the enhancement of the intensity of the net spin current. Thus, the THz radiation intensity is increased. Our findings provide a method to modulate the magnitude and polarity of THz radiation by adjusting the external magnetic field.

To summarize, we investigate the ultrafast spin dynamics of magnetized in-plane Fe/Pt (FM/NM) by THz emission spectroscopy. The polarity of THz is independent of the polarization direction of the laser beam. By changing the direction of the applied magnetic field and sample orientation, THz emission is attributed mainly to the superdiffusive transient spin current with the ISHE. The THz intensity of radiation can be modulated by varying the pump pulse intensity and the magnitude of the external magnetic field.

This work was supported by the National Key R&D Program of China (No. 2017YFA0303403), the National Natural Science Foundation of China (Nos. 11674095, 11874120, 11874015, 51671057, and 11604202), and the Shanghai Rising-Star Program (No. 18QA1401700).

## References

1. M. Massaouti, C. Daskalaki, A. Gorodetsky, A. D. Koulouklidis, and S. Tzortzakakis, *Appl. Spectrosc.* **67**, 1264 (2013).
2. R. Fukasawa, *IEEE Trans. Terahertz Sci. Technol.* **5**, 1121 (2015).
3. P. Lockhart, T. Ramotowski, and M. Rice, *Polymer Test* **34**, 140 (2014).
4. X. Xin, Y. Wu, T. Y. He, Y. Y. Li, F. R. Hu, H. S. Liang, C. X. Yang, and H. Zhong, *Chin. Opt. Lett.* **15**, 111703 (2017).
5. E. M. Pickwell, S. Y. Huang, K. W. C. Kan, Y. W. Sun, and Y. T. Zhang, *J. Innovative Opt. Health Sci.* **1**, 29 (2008).
6. T. Kohmoto, T. Moriyasu, S. Wakabayashi, H. Jinn, M. Takahara, and K. Kakita, *J. Infrared Milli. Terahz. Waves* **39**, 77 (2018).
7. J. D. Costa, T. J. Huisman, R. V. Mikhaylovskiy, I. Razzdolski, J. Ventura, J. M. Teixeira, D. S. Schmool, G. N. Kakazei, S. Cardoso, P. P. Freitas, T. Rasing, and A. V. Kimel, *Phys. Rev. B* **91**, 104407 (2015).
8. E. Hendry, M. Koeberg, J. Pijpers, and M. Bonn, *Phys. Rev. B* **75**, 233202 (2007).
9. H. Nemeč, I. Kratochvilova, P. Kuzel, J. Sebera, A. Kochalska, J. Nozar, and S. Nespurek, *Phys. Chem. Chem. Phys.* **13**, 2850 (2011).
10. M. C. Beard, G. M. Turner, and C. A. Schmittenmaer, *Phys. Rev. B* **62**, 15764 (2000).
11. D. D. Sun, M. Q. Wang, Y. Y. Huang, Y. X. Zhou, M. Qi, M. Jiang, and Z. Y. Ren, *Chin. Opt. Lett.* **15**, 051603 (2017).
12. M. Venkatesh, S. Ramakanth, A. K. Chaudhary, and K. C. J. Raju, *Opt. Mater. Express* **6**, 2342 (2016).
13. E. Beaurepaire, G. M. Turner, S. M. Harrel, M. C. Beard, J. Y. Bigot, and C. A. Schmittenmaer, *Appl. Phys. Lett.* **84**, 3465 (2004).
14. N. Kumar, R. W. A. Hendrikx, A. J. L. Adam, and P. C. M. Planken, *Opt. Express* **23**, 14252 (2015).
15. K. J. Chau, M. Johnson, and A. Y. Elezzabi, *Phys. Rev. Lett.* **98**, 133901 (2007).
16. T. Kampfrath, M. Battiato, P. Maldonado, G. Eilers, J. Notzold, S. Mahrlein, V. Zbarsky, F. Freimuth, Y. Mokrousov, S. Blugel, M. Wolf, I. Radu, P. M. Oppeneer, and M. Munzenberg, *Nat. Nanotech.* **8**, 256 (2013).
17. T. J. Huisman, R. V. Mikhaylovskiy, A. Tsukamoto, T. Rasing, and A. V. Kimel, *Phys. Rev. B* **92**, 104419 (2015).
18. W. M. Posadowski, A. Wiatrowski, K. Tadaszak, and J. Kudzia, *Elektronika* **53**, 37 (2012).
19. Y. J. Ding, *Opt. Lett.* **29**, 2650 (2004).
20. Y. Kinoshita, N. Kida, M. Sotome, T. Miyamoto, Y. Iguchi, Y. Onose, and H. Okamoto, *ACS Photon.* **3**, 1170 (2016).
21. J. N. Heyman, P. Neocleous, D. Hebert, P. A. Crowell, T. Muller, and K. Unterrainer, *Phys. Rev. B* **64**, 085202 (2001).
22. T. Seifert and U. Martens, *Spin* **7**, 1740010 (2017).
23. S. N. Zhang, Z. M. Jin, X. M. Liu, W. Y. Zhao, X. Lin, C. Jing, and G. H. Ma, *Opt. Lett.* **42**, 3080 (2017).